Phase transitions in the adsorption system Li/Mo(112)

A. Fedorus,[1] D. Kolthoff,[2] V. Koval,[1] I. Lyuksyutov,[1,3] A. G. Naumovets,[1] and H. Pfnür[2,*]
[1]*Institute of Physics, National Academy of Sciences of Ukraine, Prospect Nauki 46, UA-03039, Kyiv-39, Ukraine*
[2]*Institut für Festkörperphysik, Universität Hannover, Appelstraße 2, D-30167 Hannover, Germany*
[3]*Department of Physics, Texas A&M University, College Station, Texas 77843-4242*
(Received 29 October 1999)

Experimental studies of the phase transitions in the adsorption system Li/Mo(112) are presented. This system is a model system for highly anisotropic interactions. From measurements of the half-widths of the low-energy electron diffraction spot profiles a phase diagram is derived for the whole submonolayer region of coverage in the temperature range 100–500 K. The commensurate low-coverage phases below $\theta=0.6$ form chains normal to the troughs of the substrate. The commensurate $p(4\times1)$ phase, which is completed at a coverage, θ, of 0.25 monolayers (ML), seems to be truly long range ordered, whereas the $p(2\times1)$ phase at $\theta=0.5$ still contains domain boundaries even at the lowest temperature of 100 K. Both undergo temperature-driven order-disorder phase transitions. In contrast, the incommensurate phases existing in the coverage range $\theta=0.66$–0.90 form chains along the troughs, which are only weakly coupled normal to the troughs of the substrate. These phases exhibit two coverage-driven phase transitions from rectangular to oblique units cells and back at critical coverages of 0.66 and 0.85, respectively, and represent floating solids. As a function of temperature, they undergo a two-dimensional melting transition. Close to the critical coverages, the melting temperatures show a sharp drop below the temperature range accessible in our experiments. Both functional dependences of the angular deviation from 90° and of the melting temperature on coverage are in good agreement with a phenomenological theoretical model, assuming an instability of the shear modulus of the adsorbate unit cell at the critical coverages.

I. INTRODUCTION

Two-dimensional structures, which are subject to strongly anisotropic lateral interactions, are highly interesting because of their unique properties, which in the extreme limit can be quasi-one-dimensional. Such model systems are formed upon submonolayer adsorption on surfaces with strongly anisotropic substrate potential corrugation like (112) bcc and (110) fcc surfaces. Therefore, they have been studied by several authors (for a review, see Refs. 1 and 2). At coverages below $\theta=0.5$, chain structures of the type $p(n\times1)$ are common on these substrates with n ranging between 9 and 2. These structures consist of parallel chains of adsorbed atoms aligned perpendicularly to the substrate troughs. In the inset of Fig. 1 we show a hard-sphere model of the chain structure with $n=4$. At low temperatures, the $p(n\times1)$ structures, which are in general commensurate, can possess long-range order (if not pinned). Their existence directly demonstrates the strong anisotropy of lateral interactions. They have even different sign. In this range of coverages, the interactions along the troughs are mainly repulsive while in the perpendicular direction they are strongly attractive. The situation changes at coverages above $\theta=0.5$, where incommensurate structures form. Their incommensurate period is directed along the troughs, and coupling normal to the troughs is now much weaker than that along the troughs, as judged from an estimate of correlation lengths along these directions. Nevertheless, quasi-long-range order is still possible for these incommensurate structures.[1]

Li adsorbed on Mo(112) is just one specific example. Its structure was studied first by Gupalo *et al.*[3] We recall the succession of submonolayer structures reported by them: two commensurate structures $p(4\times1)$ and $p(2\times1)$ grow in the range of relative adatom concentrations $\theta<0.60$. At higher coverages up to $\theta=0.90$ a set of one-dimensionally incommensurate structures (1DI) was found. The correlation between rows was found to be of fairly short range, whereas long-range correlations have been seen along the rows. As a function of coverage, the intrarow spacing could be varied continuously in the range between 1.5 and 1 $a_{\overline{111}}$ ($a_{\overline{111}}$ is the

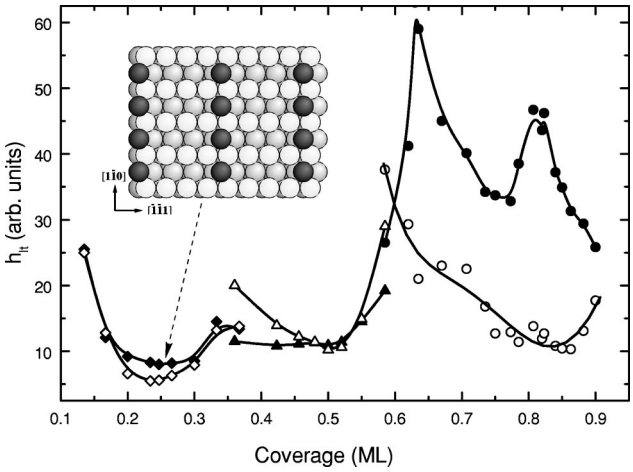

FIG. 1. Coverage dependence of the full widths at half maximum (FWHM) of LEED spots at low temperature ($T=100$ K). Full symbols are for the $[1\bar{1}0]$ direction, and the open symbols mark the $[\overline{111}]$ direction for the following structures: $p(4\times1)$ (diamonds), $p(2\times1)$ (triangles), and incommensurate structures (circles). Inset: Schematic of the real space structure (top view) of adsorbed Li on Mo(112) ordered as $p(4\times1)$ structure. The dark balls mark the Li atoms, all others are Mo atoms. Atoms with the same gray scale are located in the same layer.

lattice constant along the troughs of the substrate). The interrow spacing, however, remained fixed at one lattice constant, $a_{1\bar{1}0}$, in $[1\bar{1}0]$ direction normal to the troughs. Our low-energy electron diffraction (LEED) study corroborates most of these overall structures.

On the basis of these general data, the system Li/Mo(112) seems to be a good candidate to carry out a quantitative study of the correlational properties of such a system for both the commensurate and the incommensurate structures, and compare them directly with the well established theoretical considerations on such systems.[1] This is the purpose of our study, which has been carried out by evaluating LEED profiles for a large set of different coverages of Li on Mo(112) in a wide range of temperatures down to 100 K.

As will turn out below, the correlations in the incommensurate layers are particularly interesting, because they show a remarkable dependence on coverage with orientational changes of the ordered state. As will be shown, ordered incommensurate layers can have either rectangular or oblique unit cells, depending on coverage. Therefore, after considering the commensurate phases, we will pay special attention to the investigation of the incommensurate structures. The almost quantitative agreement of our experimental results with a phenomenological theory[4] gives insight into the possible physical origins of the behavior found experimentally, which is discussed in the last section.

II. EXPERIMENT

The experiment was performed in the μ-metal shielded UHV chamber at a base pressure of between 0.7×10^{-11} and 1×10^{-11} mbar. The experimental setup was described previously.[5] The main experimental results are obtained by measuring LEED spot profiles with a three-grid backview LEED optics and a charge-coupled device (CCD) camera. The following other methods were used: contact potential difference (CPD) monitored by a small three-electrode electron gun for coverage calibration, mass spectrometry with a quadrupole mass spectrometer, Auger electron spectroscopy using a cylindrical mirror analyzer for testing cleanness of adsorbate and substrate, and a high resolution spot profile analysis (SPA) LEED instrument for examining the structure of the substrate surface.

A molybdenum single crystal, 10 mm$\times$8 mm$\times$0.5 mm in size with (112) orientation, was used as a substrate. The specimen was cleaned in UHV by oxidation at $T=1400$ K in an oxygen pressure of 2×10^{-6} mbar for 18 h. The remaining oxygen was removed afterwards by repeated temperature cycles up to 2300 K. No carbon was detected by Auger analysis after such a procedure. The substrate structure investigated by SPA LEED showed that the average sizes of terraces in the two principal lateral directions were of $L_{\bar{1}\bar{1}1}\times L_{1\bar{1}0}=350$ Å $\times 550$ Å. The specimen could be cooled with liquid nitrogen down to 100 K and heated resistively and/or by electron bombardment up to 2500 K. The temperature was measured by a W/Re thermocouple and was controlled by a computerized feedback circuit with a resolution of 0.01 K.

The source of lithium was constructed and outgassed as described in Ref. 6. The LEED patterns have been taken mainly at an electron energy of 55 eV, which allowed the observation of the first Brillouin zone at sufficiently high intensity. The instrument transfer width of the backview LEED system is 2% of the substrate Brillouin zone (BZ) in the $[\bar{1}\bar{1}1]$ direction and 3.5% in the $[1\bar{1}0]$ direction at this energy.

Coverage was calibrated by measuring the work function change as a function of coverage and the intensities of the LEED superstructures. The maximum LEED intensities of the $p(4\times1)$ and $p(2\times1)$ structures have been identified with the coverages 0.25 and 0.5. After this calibration, relative coverages were determined only from the work function data. For coverages higher than 0.65 the incommensurate lattice constant was used directly for coverage determinations.

From the original data a background was subtracted, which was determined at the location between the diffraction spots, and linearly interpolated. Obvious distortions due to the grids have also been corrected for. Where peak intensities have been used to show qualitative trends, we determined them as the average over typically 10 pixels on the screen. Taking the approximately Gaussian shape of the integral order beams as instrument function, the full widths at half maximum (FWHM's) of the superstructure beams have been determined by deconvolution. For quantitative estimates of domain sizes, we took the inverse FWHM after deconvolution. This value corresponds to twice the correlation radius, R_c.

III. RESULTS

A. Low-coverage region: commensurate structures

1. Structures as a function of coverages at T=100 K

First, faint spots of the $p(4\times1)$ structure appear after Li deposition (at low temperature and subsequent annealing) at a coverage $\theta=0.1$. During further increase of coverage, the $p(4\times1)$ features grow in intensity and sharpness, but the FWHM of these spots reaches the instrumental width only close to the completion of $p(4\times1)$ at a coverage of 0.25. A similar growth in intensity and sharpness of LEED spots is observed for the $p(2\times1)$ structure when coverage gets close to its stoichiometric value of 0.5. Beyond these ''ideal'' coverages, h_{lt} is not only broader, but also shows some anisotropy, though not very large. Such a behavior is indicative for an island and/or antiphase domain growth mode, as found in many other systems, e.g., for O/W(011) (Refs. 7–9) and O/W(112) (Refs. 8 and 10). Figure 1 shows the coverage dependence of the low-temperature FWHM, h_{lt}, for the $[\bar{1}\bar{1}1]$ and $[1\bar{1}0]$ directions. The increase of h_{lt} can be connected with a reduction of island sizes on the low-coverage side of each structure, but also with the creation of new domain walls, especially if coverage exceeds the optimal value, possibly due to nucleation of islands with different structure.

As coverage reaches the values $\theta=0.25$ and $\theta=0.5$, corresponding to completion of the $p(4\times1)$ and $p(2\times1)$ structures, h_{lt} reaches its minimum values (see Fig. 1) and the spots are almost round. Especially the $p(4\times1)$ structure seems to reach undistorted long-range order for the completed structure since the FWHM in $[\bar{1}\bar{1}1]$ direction corresponds to the instrumental width. In the perpendicular direc-

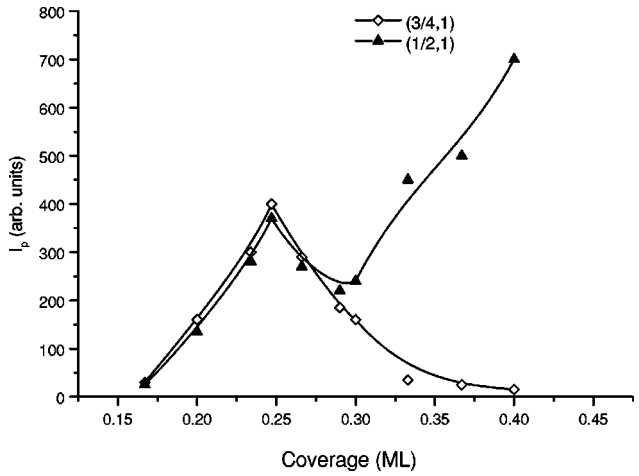

FIG. 2. Coverage dependence of the peak intensity of the ($^1/_2$,1) and ($^3/_4$,1) LEED spots at low temperature ($T=100$ K).

tion, i.e., normal to the troughs of the substrate, however, domain walls seem to be frozen in, as evident from the half-width, which is about 1.5 times as large in the $[1\bar{1}0]$ direction compared with the $[\bar{1}\bar{1}1]$ direction. An even higher density of domain walls in both directions has to be concluded from Fig. 1 for the $p(2\times1)$ structure at 100 K, which limits the average domain size of this structure in its best ordered state to 50 Å . This corresponds to a domain wall density of about 4×10^{12} cm^{-2}.

The evaluation of the FWHM's alone leads to ambiguities in the transition region between the $p(4\times1)$ and $p(2\times1)$ structures, because the superstructure spots of the $p(2\times1)$ are a subset of the $p(4\times1)$ structure. Therefore, peak intensities of superstructure spots have been measured. In Fig. 2, the peak intensities of the ($^3/_4$,1) spot, existing only for the $p(4\times1)$ structure, and of the ($^1/_2$,1) spot, common for both $p(4\times1)$ and $p(2\times1)$ structures, are plotted. As seen from this figure, the behavior of these spots as a function of coverage starts to deviate at a coverage of 0.29, indicative for the beginning formation of $p(2\times1)$ islands, which coexist with $p(4\times1)$ islands up to a coverage of close to 0.40. Here the intensity of spots corresponding to the $p(4\times1)$ structure can no longer be discriminated from the background intensity. The upper limit of existence of the $p(2\times1)$ structure was found at $\theta=0.59$. Up to this coverage, the only ordered structure is a (rather diffuse) $p(2\times1)$ structure, whereas at higher coverages incommensurate ordered overlayers are formed.

Summarizing this first overview of the commensurate structures in this system at low temperature (100 K), the region $0.29<\theta<0.37$ is occupied by the two coexisting phases $p(4\times1)$ and $p(2\times1)$. In the adjacent coverage ranges, single phases $p(4\times1)$ and $p(2\times1)$ exist, respectively. Only the lattice gas exists at coverages below 0.1.

2. Profile widths as a function of temperature

Figure 3 shows the temperature dependence of the half-widths measured for the $p(4\times1)$ and $p(2\times1)$ structures, respectively. The data are given for both the $[\bar{1}\bar{1}1]$ and $[1\bar{1}0]$ directions. The transition is reversible, as tested by temperature sweeps back and forth. This property is a necessary, but not sufficient, indication that the transitions might be of second order. While the resolution of the instrument used here is not good enough to carry out a precise quantitative analysis, which would be necessary in order to make a safe conclusion about the order of the phase transition, we make some brief remarks on the possible implications of first- or second-order phase transitions. Second-order transitions would result in a decay of the correlation length of critical fluctuations $\propto(T-T_c)^{-\nu}$, i.e., a broadening of the spots measured by the half-width $\propto(T-T_c)^{\nu}$. For continuous order-disorder transitions these transitions should belong to the universality classes of the four-state Potts model and the Ising model, respectively,[1,11] in which the critical exponent ν has the value 0.66 (four-state Potts) and 1 (Ising). In principle, chirality should be relevant in uniaxial systems like the one investigated here.[12] In this case, however, the creation of domain walls above T_c should result in a continuous shift of the peak positions of diffraction peaks.[12] This was not observed. All superstructure spots of both $p(4\times1)$ and $p(2\times1)$ structures remain at fixed positions also during disordering. On the other hand, also for a weak first-order transition hysteresis can be arbitrarily small and not visible in experiment. It would be coupled with finite, but large fluctuations, which scale with an effective critical exponent $\nu=0.5$.[13]

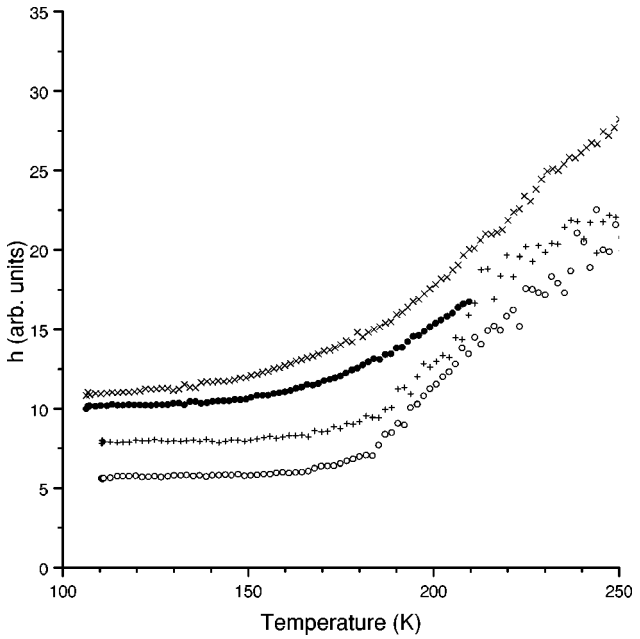

FIG. 3. Temperature dependence of FWHM of the ($^3/_4$,1) LEED spot from the $p(4\times1)$ structure (+ and ○) and that of the ($^1/_2$,1) LEED spot from the $p(2\times1)$ structure (× and ●). + and × are for measurements in $[1\bar{1}0]$ and circles for measurements in $[\bar{1}\bar{1}1]$ directions, respectively.

As seen from Fig. 3, the half-width of the $p(4\times1)$ structure shows indeed a sublinear increase of the FWHM starting at 185 K. If this temperature is used as T_c, an effective critical exponent $\nu=0.8\pm0.1$ is obtained, which is not very far from that expected for the four-state Potts universality class. This result may be taken as an indication for a second-order transition to disorder in a perfect system. However, the existence of several domains on each substrate terrace indicates that the system is far from ideal, and that the ordering

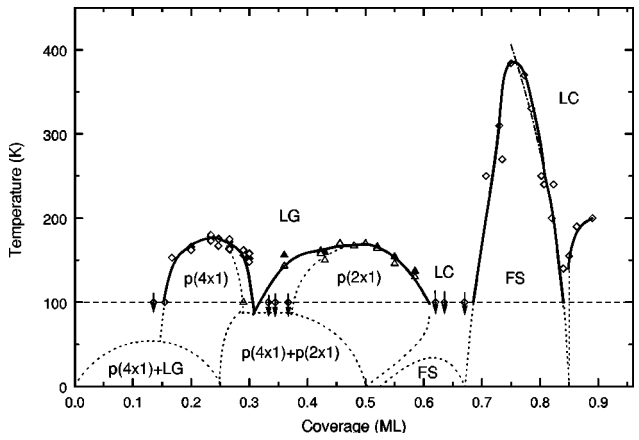

FIG. 4. Phase diagram of the Li/Mo(112) system. LG: lattice gas; LC: liquid crystal; FS: floating solid. Dashed lines show suggested phase boundaries. Dash-dotted line shows an approximation of the phase boundary by the square-root law (see text).

process at low temperature is dominated by defects like step edges.

For the completed $p(2\times1)$ structure, it turns out that it is very difficult to define a critical temperature exactly even at a coverage of 0.5. The pronounced smearing of the transition might be caused by the high defect density incorporated already in the ordered structure. A linear increase in half-width can be observed over a wide temperature range above 200 K. The situation in general is thus similar to the $p(4\times1)$ structure. Nevertheless, it is remarkable that this structure contains an even higher density of extended defects than in the $p(4\times1)$ structure.

This high defect density might also be the reason for the observation of a slight increase of the FWHM as a function of T already below the average T_c (for its definition, see below), which was not found in the $p(4\times1)$-ordered phase or in many similar systems possessing long-range order, e.g., $p(2\times1)$O/W(112).[14] This peculiarity seems to manifest typical properties of an inhomogeneous system consisting of many small ordered domains. Since there is a distribution of domain sizes, thermal excitations specific of chain structures, namely, displacements of the chain sections from the potential wells aligned along the base chain line to those adjacent,[15] are able to disorder the various domains at different temperatures, which ''smears'' the phase transition. Clearly, the process of kink formation in the originally straight chains corresponds to just the formation of domain walls. The size of still straight sections is governed by temperature and interaction energy parameters. Since the $p(4\times1)$ structure appears at an earlier stage of submonolayer growth than $p(2\times1)$, the latter is characterized by a smaller interaction energy ε_1. This might be a reason why domains can be more easily created, but also more easily pinned and frozen in.

3. Phase diagram, low-coverage section

In order to derive a phase diagram, linear interpolations of the constant and the increasing sections of the half-widths have been constructed for different coverages, and the points of intersection have been used as critical temperatures. Figure 4 shows a summary of all characteristic changes of half-widths, which are taken as the respective critical temperatures and plotted as a function of coverage. The measured phase boundaries are presented by solid lines, their suggested extrapolations by dotted lines.

The phase boundary shows two maxima at coverages $\theta=0.25$ and 0.5 for the $p(4\times1)$ and $p(2\times1)$ structures, respectively. The maximum critical temperatures derived from these points are nearly equal for both structures. The equality of the critical temperatures is consistent with the consideration that the essential step towards disordering of any chain structure is the decomposition of the chain.[15] The corresponding binding energy, ε_0, is much larger than the energy of the interchain interaction, ε_1.[2] Under this condition, following Ref. 15, $T_c \propto \varepsilon_0$, whereas T_c depends only logarithmically on ε_1. Therefore, the obtained value of T_c can be used for a rough estimate of the in-chain binding energy, which gives $(1.6\text{–}3.4)\times10^{-2}$ eV (Ref. 15) if we assume a ratio T_c/ε_1 between 10 and 100. The Ising model in an approximation of only nearest-neighbor interactions, which also can be applied to the order-disorder transition in the $p(2\times1)$ structure, gives a similar value $\varepsilon_0=1.76T_c=2.6\times10^{-2}$ eV. A recent Monte Carlo simulation[16] of the previously measured temperature dependence of the peak intensity for $p(4\times1)$ structure[3] resulted in $\varepsilon_0=2\times10^{-2}$ eV, which is consistent with our result. As found from a comparison of the FWHM values for the two directions at $T>T_c$, no remarkable anisotropy appears upon disordering.

The critical temperature decreases roughly quadratically with the coverage deviation from the values $\theta=0.25$ and 0.5 in their vicinity. A sharp decrease of the $p(4\times1)$ order-disorder curve is found for $\theta\approx0.15$ and $\theta\approx0.3$. The corresponding plots $h(T)$ do not show any characteristic onsets of increasing half-widths beyond this range. Evidently, the transition temperatures shift below those accessible in the present experiment (shown by arrows pointing downwards in Fig. 4). It is possible that the sharp decrease of T_c at $\theta=0.15$ marks the transition to a broad two-phase region consisting of a lattice gas (LG) and $p(4\times1)$ islands at temperatures lower than those accessible in our experiment, taking into account the conclusion of Ref. 17. This coexistence region $p(4\times1)+$ LG is indicated as dotted line in Fig. 4.

Further details of the phase diagram can be derived, if we again consider FWHM's at various coverages, and in particular their temperature dependence. While the half-widths of the $p(4\times1)$ single phase formed at $\theta=0.25$ stay at a nearly constant value below T_c, the low-temperature section of the $h(T)$ plot shows a noticeable slope as coverage deviates from $\theta=0.25$ by $-0.09/+0.04$. From the larger half-widths at these coverages already at the lowest temperature compared with $\theta=0.25$ we conclude that there might be numerous domain walls on the low-coverage side, and a small range of coexistence between $p(4\times1)$ ordered islands and a fluid at the high coverage side. This fluid may already contain $p(2\times1)$ correlations. The quickly varying density of the disordered phases as a function of temperature above 100 K has a direct consequence on the size of the $p(4\times1)$ ordered islands. By increasing temperature, the equilibrium concentration of the $p(4\times1)$ ordered phase decreases. If the number of islands stays constant, the average size must decrease below complete disordering, as seen in our experiments.

The sharp decrease of T_c at $\theta=0.3$ marks the end of the $p(4\times1)$ phase (coexisting with a fluid phase). At higher coverages, we found (see Fig. 2) coexistence between $p(4\times1)$ and $p(2\times1)$ islands at temperatures above 100 K in the coverage range up to 0.37. As suggested by symmetry arguments, we speculate that this range of coexistence might be extended over the whole range of coverages down to 0.25 and up to 0.5 at temperatures lower than 100 K. The low-coverage branch of this coexistence line *above* 100 K starts at a coverage of 0.29, and the high-coverage branch ends at a coverage of 0.37, as found experimentally.

With all these details included in the phase diagram, the discussed portion of the phase diagram has the typical form of that of eutectic alloys. Using the alloy terminology, the high-temperature phase boundaries of our phase diagram between the coverages 0.25 and 0.5 mark the liquidus lines and the point $\theta=0.3$, $T<100$ K an eutectic point. The solidus lines can only be marked schematically, since no clear transitions can be identified. A eutectic mixture of the two solid phases $p(4\times1)$ and $p(2\times1)$ may exist in the coverage range of $\theta=0.29-0.37$ at $T<100$ K. What we are able to observe above 100 K is only the coexistence of one solid with one liquid component. The high-coverage part of the phase diagram will be discussed below.

B. High-coverage region: Incommensurate structures

1. Coverages $0.50<\theta<0.66$

No coexistence of commensurate and incommensurate structures is observed at $T>100$ K in the coverages range $0.50<\theta<0.66$. Instead, at coverages slightly above $\theta=0.50$ and at the lowest temperature available in our experiment, the LEED features of a $p(2\times1)$ structure gradually deform and broaden, transforming eventually into those specific for an incommensurate structure [see Fig. (5)]. At the first stage, the $(^1/_2,k)$ spots are elongated in $[\overline{1}11]$ direction (see Fig. 5b) indicating an increase in the density of domain walls perpendicular to the troughs. At $\theta=0.59$, the domain size $L_{\overline{1}11}$ (which can be estimated from the data of Fig. 1) is reduced to a value corresponding to 3–4 periods of the $p(2\times1)$ lattice. Above a coverage of 0.60, broad superstructure spots are observed [Fig. 5(c)], which can be attributed neither to $p(2\times1)$ nor to the new $p(1.5\times1)$ structure (see below). Finally, close to $\theta=0.66$, spots specific for a $p(1.5\times1)$ structure form [Fig. 5(d)].

The LEED pattern $p(1.5\times1)$that corresponds to the beginning of the incommensurate region does not uniquely determine the adatom arrangement at $\theta=^2/_3$. A model of a one-dimensionally incoherent structure discussed earlier[3] seems to be ruled out because of the shape of diffraction spots: though elongated, they are not totally spread into streaks. The geometrical model shown in Fig. 6(a), which is characterized by the uniform spacing between adatoms along the trough, would be appropriate if no corrugation caused by variations of the adsorbate-substrate potential, $E_{ads-sub}$, along the troughs exists. This is of course an extreme case. However, any possible substrate-induced relaxations due to $E_{ads-sub}\neq0$ are not correlated along the troughs, since they do not introduce any superperiodicity in this direction. On the other hand, such relaxations might be the reason for adatom correlations in different troughs with changing average direction of correlation as a function of adatom density (see below).

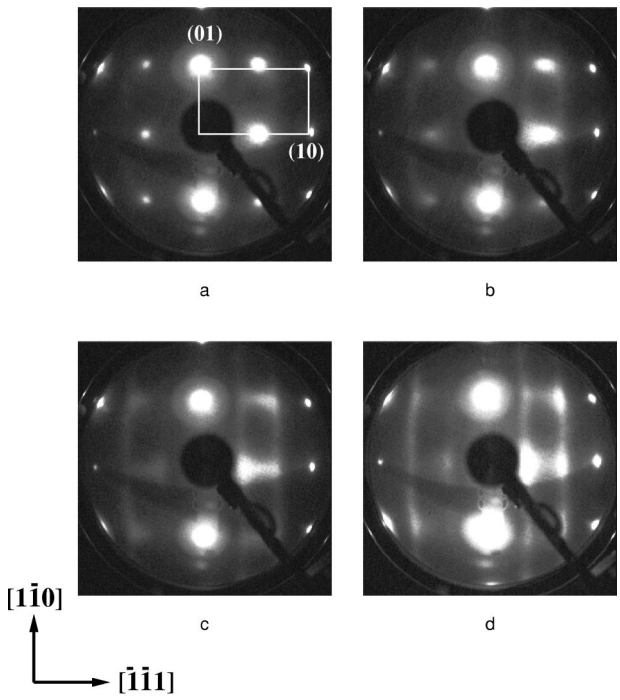

FIG. 5. LEED patterns observed at low temperature in the region of transition from commensurability to incommensurability: (a) $\theta=0.55$; (b) $\theta=0.585$; (c) $\theta=0.62$; (d) $\theta=0.635$. The unit mesh of the substrate is also shown. (10) corresponds to the $[\overline{1}11]$ direction, (01) to the $[1\overline{1}0]$ direction.

2. Orientational phase transitions $(0.66<\theta<0.85)$

Beginning at a coverage of 0.66, the superstructure spots of the incommensurate layer continuously shift towards the integral order beams in $[\overline{1}11]$ direction. This shift turned out to be inversely proportional to the lattice constant of the overlayer. No further modulation of the beam profiles have been found in this direction. In addition, the superstructure spots start to split in the $[1\overline{1}0]$ direction, as shown in the middle panel of Fig. 7. This splitting is a continuous function of coverage and reaches a maximum at a coverage of 0.74. It decreases again at higher coverages and vanishes for coverages above $\theta=0.85$. This splitting is due to the formation of incommensurate oblique unit cells in the adsorbate, as also indicated in Fig. 7, in contrast to the rectangular unit cells at coverages below $\theta=0.66$ and above $\theta=0.85$. Two rotational

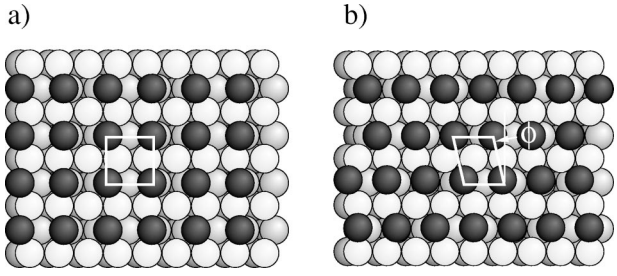

FIG. 6. Suggested models of incommensurate structures for: (a) $\theta=0.66$; (b) $\theta=0.75$.

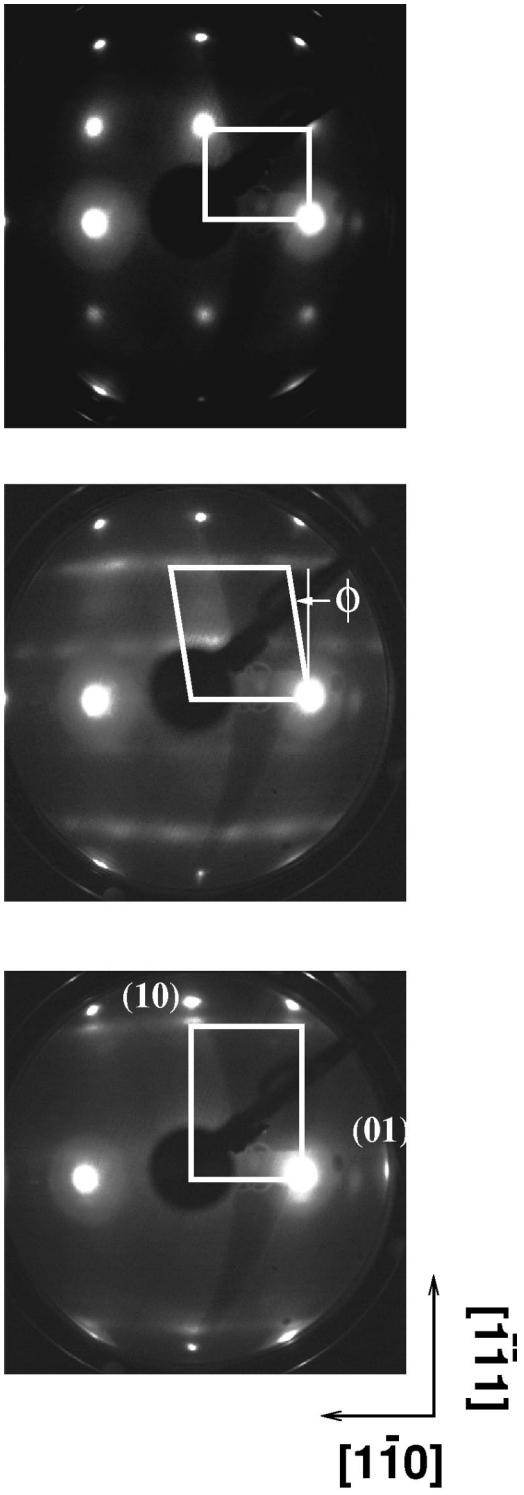

FIG. 7. LEED patterns for the incommensurate phase obtained at coverages 0.75 (middle) and 0.90 (bottom). For reference, also the commensurate $p(2\times1)$ phase at $\theta=0.5$ is shown atop. These patterns demonstrate the transition from rectangular unit cells to an oblique cell and back, as indicated by the reciprocal unit cells drawn.

domains of the oblique structures can be formed. A hard-sphere model of the real space structure with an oblique unit cell close to the maximum angular deviation from a rectangular cell at a coverage of 0.75 is shown in Fig. 6(b). It is clear that from the LEED patterns only the average distances and angles can be determined.

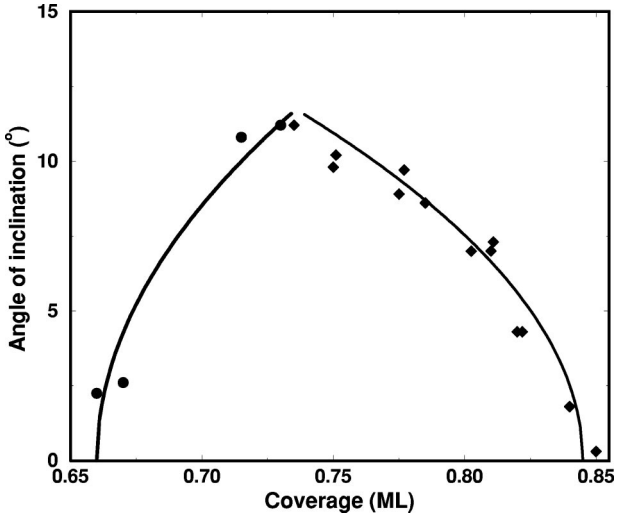

FIG. 8. Deviation, ϕ, of the angle between the axes of the unit cell from rectangular as a function of coverage. The lines indicate the functional dependence $\phi\propto\sqrt{|\theta-\theta_c|}$ with critical coverages $\theta_c=0.66$ and 0.845, respectively.

This finding is evidence for a second-order transition between rectangular and oblique structures driven by the concentration of adsorbed Li atoms. The angular deviation from 90°, ϕ, of the angle between the axes of the incommensurate unit cells can easily be determined from the observed splitting (see Fig. 8). These data can in fact be interpreted as two continuous orientational phase transitions: at a coverage of 0.66 from a rectangular to an oblique unit cell, and a similar one, but now as a function of *decreasing* coverage at $\theta=0.85$.

The formation of incommensurate structures is coupled with an appreciable anisotropy of the half-width and therefore of the correlations within the film. The data on low-temperature FWHM are presented in Fig. 1. Indeed, in contrast to the commensurate structures, for which the values obtained in $[\overline{1}11]$ and $[1\overline{1}0]$ directions are almost identical, they are remarkably anisotropic for the incommensurate structures in the whole region of incommensurability. Slightly above a coverage of 0.66, the $p(1.5\times1)$ spots are already elongated in the $[1\overline{1}0]$ direction, i.e., perpendicular to the elongations just described for the transition from $p(2\times1)$ to incommensurate structure. No true long-range order can be observed at this coverage. From the half-widths at $T=100$ K, we estimate correlation lengths of 8 and 3 lattice constants in the $[\overline{1}11]$ and $[1\overline{1}0]$ directions, respectively. This indicates the new anisotropy in coupling parallel and perpendicular to the troughs not found at lower coverages. For the $[\overline{1}11]$ direction, h_{lt} decreases gradually with coverage until coverage reaches $\theta=0.85$. In this range of coverage, the correlation length rises from 8 to 14 spacings. For the $[1\overline{1}0]$ direction, h_{lt} is 2–4 times as large, so that correlations exist only over typically 3–4 lattice spacings. Moreover, a complicated nonmonotonic variation of the half-widths is observed for this direction, showing a minimum at $\theta=0.75$.

It is worth noting that in the region of compression, coverage passes through the rational as well as irrational values. The ground state of such an overlayer is considered as an

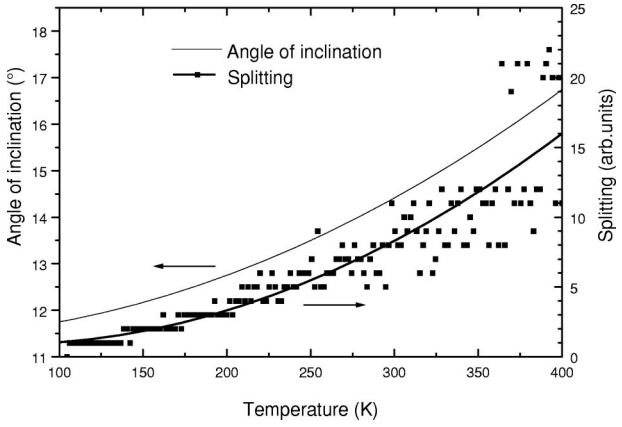

FIG. 9. Temperature dependence of splitting at $\theta = 0.735$.

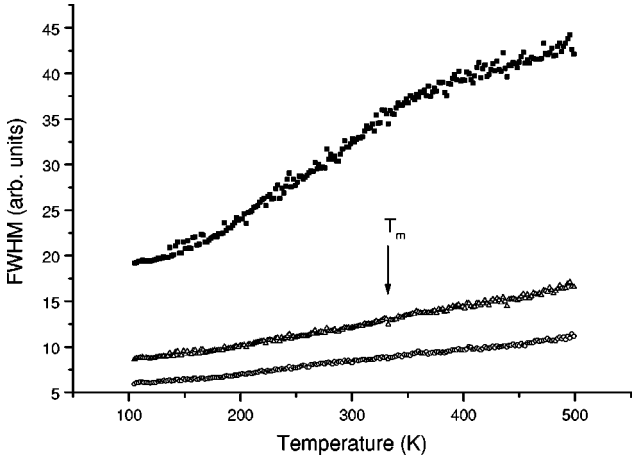

FIG. 10. Temperature dependence of the full widths at half maximum of the $(-0.785,-1)$ LEED spot from the incommensurate structure ($\theta = 0.785$) measured in the following directions: $[1\bar{1}0]$ (full squares), $[\bar{1}11]$ (circles), and their root mean square average (triangles). The melting temperature is indicated by an arrow.

infinite set of commensurate and incommensurate phases (devil's staircase, which is defined[1] as a hierarchy of commensurate lattices with infinitely increasing order of commensurability). In particular, the models presented in Fig. 6 correspond to the rational values of coverage and could fall into a commensurate class. However, long-range order specific for such commensurate phases is realized only below the pinning temperature,[1] which was never attained in our experiment. All the structures observed in the region of compression possess either quasi-long-range order or only short-range order.

As just demonstrated, the incommensurate layers with oblique unit cells have especially weak coupling in the direction normal to the troughs. Nevertheless, the results shown in Fig. 8 depend very weakly on temperature, as explicitly tested. As a rule, the initial anisotropy of the FWHM characteristic for the incommensurate films at low temperature does not vary noticeably with temperature. Exceptions are found near the edges of the region of the oblique-lattice existence where the ratio $h_{1\bar{1}0}/h_{\bar{1}11}$ increases by 25–35 % upon heating. It is worth noting that the skew angle also varies slightly with temperature. This is shown in Fig. 9 for the largest angles of deviation from a rectangular configuration, ϕ, around $\theta = 0.75$. The temperature-induced changes were found to be 10^{-2} deg per kelvin over the temperature range from 100 to 400 K. This temperature dependence of ϕ shows that the incommensurate layers represent indeed a floating solid. It cannot be explained by thermal expansion of the substrate, from which an influence about 2 orders of magnitude smaller should be expected. We will discuss these findings below within the framework of a phenomenological theory and simple microscopic considerations.

3. Coverages $0.85 < \theta < 0.90$

With further increase of coverage after the transition back to a rectangular lattice, one-dimensional compression of the incommensurate adatom row in each substrate trough is observed up to $\theta = 0.90$ (physical monolayer which is not strained, i.e., the density in each row corresponds to the Li crystal density). As a function of coverage the unit cell stays rectangular, and the degree of FWHM anisotropy decreases when approaching the physical monolayer (see Fig. 1). In this coverage range, the coverage determined from the ratio of substrate to adsorbate spacing, $a_{\bar{1}11}/b_{\bar{1}11}$, along the trough by LEED and the relative concentration determined from the deposition time are in full agreement. According to these results, the highest density obtained in the monolayer corresponds to a value of $a_{\bar{1}11}/b_{\bar{1}11} = \theta_1 = 0.90$. At $\theta > 0.90$, the structures observed are characteristic of $a_{\bar{1}11}/b_{\bar{1}11}$ less than the value determined from the deposition time. Therefore they are attributed to formation of the second layer.

4. Phase diagram, high-coverage part

A series of temperature-dependent FWHM's has been measured at various (constant) coverages in the region of compression. Figure 10 shows a typical example of curves obtained. Besides the individual data for the $[\bar{1}11]$ and $[1\bar{1}0]$ directions, the data-averaged root mean squares, $\tilde{h}(T)$, are also presented in this figure. The main difference of the plots shown in Fig. 10 from those given above for the commensurate structures consists in the absence of a low-temperature leveling off. At low temperature, the majority of such plots have a slightly concave shape. To find out the character of order, we simulated an experimental spot profile by convolution of the structure factor $I(q) \propto |q|^{-2+\eta(T)}$, typical of quasi-long-range order[1] (q is the momentum transfer, η the critical index of the anomalous dimension), with the instrument transfer function assumed to have Gaussian form. The width of the instrument function was estimated from the smallest half-widths of integral order spots. The resulting curve possesses a shape close to the experiment in the reasonable range of η between 0 and 1. Therefore, we conclude that the low-temperature segment of most of the measured plots is consistent with quasi-long-range order. In many plots (particularly for $\theta > 0.67$) a point of inflection can be identified at the transition from a weak concave dependency at low temperature to a stronger convex one at high temperature. This feature is taken as evidence of complete melting of a floating solid, since theory[1] predicts an exponential decay of the correlation radius near the melting point T_m as $R_c \propto \exp\{\text{const} \times [T_m/(T-T_m)]^{1/2}\}$. This dependence gives $h(T)$ a convex shape. Inflection is more pronounced for the

$[1\bar{1}0]$ direction, but the experimental data also show more scatter for this direction. Therefore, the directionally averaged data were considered as most reliable for the determination of the melting point. There are some plots showing no inflection point, e.g., those for θ between 0.62 and 0.67. These curves are interpreted to undergo melting below the lowest working temperature of our experiment.

The melting temperatures derived from inflection of the $\tilde{h}(T)$ curves for the incommensurate structures are plotted in Fig. 4. The resulting curve constitutes a phase boundary between a floating solid and liquid. The boundary forms a pronounced maximum exactly at the coverage that corresponds to the maximum angle of inclination of the unit cell, ϕ. On the low-coverage side, the phase boundary drops sharply below 100 K, probably to zero temperature. A similar drop can be seen on the upper-coverage edge as well.

Thus the phase diagram is obtained for the incommensurate Li film adsorbed on Mo(112), which not only manifests a basic property of two-dimensional crystals, quasi-long-range order, but also reveals peculiarities specific for the highly anisotropic interactions: a transition from a rectangular to oblique lattice and a substantial drop of the melting temperature upon this transition.

IV. DISCUSSION

The phase diagram and the phase transitions in this system are governed by a remarkable change of the underlying microscopic lateral interactions. These we will discuss first, before we try to couple them with a phenomenological macroscopic description.

The chain structures formed at coverages up to $\theta=0.5$ are dominated by strong attractive interactions along the chains normal to the troughs of the substrate, whereas the interactions along these troughs are comparatively weak.[15] These commensurate structures show small anisotropy with comparable correlation lengths in both directions. They grow with wide regions of coexistence between lattice gas and $p(4\times1)$ phases, and between $p(4\times1)$ and $p(2\times1)$ phases, respectively. This is in accordance with a concept[2] that adatom interactions mediated by the substrate dominate in both directions at these adatom densities. In fact, the appearance of just the $p(4\times1)$ structure can be ascribed to lateral interactions that are caused by the local distortion of the electron density of the substrate due to the adsorbed Li atoms. This distortion is screened in an oscillatory way, and causes an oscillatory interaction potential with a periodicity of $2k_F$ (Ref. 18) (k_F is the wave vector at the Fermi energy). This low-density adsorption is coupled with a large dipole moment of the Li atoms (though no real ionic bond is formed[18]) associated with a large change in work function. The strong coupling within the chains also causes a small diffusion coefficient compared with coverages above $\theta=0.5$, mainly due to the high activation barrier that is necessary to break the chains in order to allow diffusion of single atoms.[19] A model similar to that just described has been used in a model study of this system at low coverage,[20] which correctly describes some aspects of phase diagram up to $\theta=0.5$.

The coverage of 0.5 marks a turning point in many respects for this adsorption system. The work function change has its minimum value there for the first monolayer, which is normally taken as the indication of the transition from a more ionic to a metallic bond.[2] In addition, the nature of the lateral interactions begins to change at this coverage, as indicated above, making the formation of small domains more likely than at smaller coverages. These properties are coupled with the beginning of a strong increase of the measured diffusion coefficients.[19]

The incommensurate structures observed at high coverages ($\theta>0.66$) provide the best indication that the nature of lateral interactions has completely changed compared with the low-coverage commensurate phases. The possibility to continuously change the lattice constant with Li density and the direct proportionality of inverse lattice constant and density show that the lateral interactions along the troughs are now dominated by direct repulsion between the adatoms. The high density of adatoms in rows results in a partial loss of the substrate-mediated exchange bonds across the troughs because not all adatoms in rows can occupy the optimal adsorption sites providing substrate mediation. This obviously causes a drastic weakening of coupling in $[1\bar{1}0]$ direction so that complete rows of Li atoms in the individual troughs can be shifted against each other rather easily. This property can also be described in terms of a phenomenological continuum theory as the decrease of the shear modulus in these layers. This will be discussed below.

It may not be surprising that also many properties of the diffusion coefficient are correlated with this change of lateral interactions at high Li coverages. It is interesting to note that the transition from commensurate to incommensurate phases manifests itself in a strong growth of Li diffusivity on Mo(112).[19] This growth sets in pronouncedly just above $\theta=0.5$, when the local incommensurate areas (antiphase domain walls or solitons) start to emerge in the adlayer, and continues up to $\theta=0.90$. It was estimated that at $T=300$ K the diffusivity in this coverage range increases by about four orders of magnitude. This observation indicates that, on the whole, the surface potential corrugation becomes much smoother in the commensurate to incommensurate transition. This may be due both to enhancement of the repulsive lateral interactions and to weakening of the coupling of Li adatoms within the chains while passing to the incommensurate phase. Obviously, this should facilitate the operation of a collective diffusion mechanism, in particular, of the soliton mechanism.

As just mentioned, the most interesting and surprising result of this study is the observation of continuous phase transitions from a rectangular to an oblique phase and back. This effect can be considered as one of the manifestations of so-called orientational phase transitions. In such transitions, the crystal axes of the overlayer change their orientation abruptly or gradually with respect to the axes of the substrate as the interatomic distance in the incommensurate layer varies with coverage.[21] The driving force here is an attempt of the overlayer to ensure for adatoms as many energetically favorable positions on the substrate as possible in order to minimize the free energy. In the case of Li on Mo(112), the peculiarity of the orientational phase transition is determined by the strong substrate anisotropy: the substrate keeps one of the overlayer axes fixed (that oriented along the channels) while the other can rotate continuously.

This orientational phase transition can only be understood

by the change to rather weak coupling between the rows of Li atoms, and a correspondingly low shear modulus of the layer. We now try to explain this phenomenon within the framework of a phenomenological theory for a strongly anisotropic, elastically coupled system in two dimensions,[4] which is in full agreement with the results of our experiments. In this phenomenological model, only particle motion along the troughs is allowed, and the corrugation within the troughs is ignored. Continuous phase transitions from rectangular to oblique phases can occur.

As shown in Ref. 4, if a continuous phase transition from a rectangular to an oblique unit cell happens, the shear modulus, according to Landau theory, must undergo an instability, $K_2 \propto (\theta_0 - \theta)$, where θ_0 is the coverage which corresponds to the transition point from the rectangular to the oblique structure at $T=0$. Above θ_0, i.e., in the oblique phase, the angle between the axes of the unit cell becomes coverage dependent and deviates from 90° by $\phi \propto \sqrt{\theta_0 - \theta}$. By formally changing the sign of the terms that contribute to the Landau free energy as a function of ϕ, the transition as described can also occur with decreasing coverage.

The proposed coverage-driven mechanism of instability of the shear modulus suggests a weakening of the effect in the coverage regions where the adsorbate to substrate spacing ratio closes to integers. In this particular system, approaching of θ to 1 could cause repairing of orthogonal coupling. Indeed, maximum obliquity and correlation anisotropy are observed at $\theta \approx 0.75$, the value equally far from those corresponding to the nearest simple adsorbate to substrate spacing ratio, i.e., 0.5 and 1; a back rectangular/oblique transition is found at $\theta = 0.85$ and correlation anisotropy fades with reaching a monolayer, i.e., while θ closing to 1.

It turns out that two melting mechanisms are possible.[4] One is the dislocation-mediated melting with the transition temperature. In this case, $T_m \propto \sqrt{\theta_0 - \theta}$. The second mechanism is an Ising-like transition due to formation of antiphase domains with different sign of the skew angle. This transition corresponds closely to a standard order-disorder phase transition. It was found that the transition temperature for the Ising-like melting transition in the limit of small $(\theta_0 - \theta)$ is given by

$$T_I = \propto \frac{\sqrt{\theta_0 - \theta}}{\ln(1/\theta_0 - \theta)}. \tag{1}$$

So both melting mechanisms lead essentially to the same coverage dependence, but not at the same temperatures. From our experiments, we can test the coverage dependences of both the angle of inclination of the unit cells, ϕ, as a function of coverage, and, with rather large error bars, the coverage dependence of the melting points as identified above.

Whereas on the low-coverage side there are not enough data points for ϕ to test agreement with the theoretical model outlined above, a test is possible at coverages between 0.74 and 0.85. The dash-dotted line drawn in Fig. 4 for this range of coverage corresponds to a best fit of the data to a square-root dependence of ϕ on (decreasing) coverage with a critical coverage $\theta_0 = 0.845$. This line shows that our data are in close agreement with the prediction of theory. Also data at lower coverage are compatible with a square-root dependence of ϕ on coverage with a critical coverage of 0.66. This agreement shows that we can indeed interpret our experimental findings concerning the changes from rectangular to oblique unit cells as an instability in the shear modulus of the rows of Li atoms along the troughs at coverages 0.66 and 0.85.

This conclusion is also in agreement with the temperature dependence of the half-widths of the incommensurate superstructure spots. Clear points of inflection in the FWHM could only be identified in the coverage range between $\theta = 0.70$ and 0.83. As mentioned, at coverages lower than 0.70 and higher than 0.83 the phase boundary drops sharply below 100 K, probably to zero temperature. This is fully compatible with the occurrence of an instability, as suggested by theory.[4] The dependence of the melting temperature on coverage drawn in Fig. 4 by the dash-dotted line for coverages above 0.75 again agree with the prediction of the theory outlined above of $T_m \propto \sqrt{\theta_c - \theta}$. Its functional form fits the same critical coverage, $\theta_c = 0.845$, as that used above for the angles of inclination. At this coverage, T_m should drop to zero. Since the uncertainties in the determination of T_m are rather large, and temperatures below 100 K were not accessible, only compatibility with theory can be shown.

V. CONCLUSIONS

To conclude, we have studied the phase diagram and the phase transitions of an alkali metal on a highly anisotropic substrate. The phase diagram of the low-coverage phases resembles very much those of two-component alloys. The alloy in this case consists of Li atoms and vacancies. This implies site specific adsorption up to a coverage of 0.5. The lateral interactions are characterized by strong (attractive) coupling normal to the troughs of the substrate, and an interaction along the troughs that is compatible at low coverages with that caused by screening of the charge distortion due to the adsorbed Li atoms.

Combined with the transition from commensurate to incommensurate structures at a coverage of 0.5, the interactions are now dominated by direct repulsion between the Li atoms along the troughs and a comparatively weak coupling in orthogonal direction. This type of interaction leads to a new type of phase transition in the incommensurate two-dimensional lattice. Due to highly anisotropic interactions, the oblique lattice is stable in a broad range of coverages. This results in two transitions between these two types of lattices at critical coverage of 0.66 and 0.845, respectively. The quantitative behavior of these transitions agrees well with a model assuming that the shear modulus of the layers tends to zero at the critical coverages. The strong decrease of the shear modulus at these coverages results in the development of smecticlike fluctuations of the rectangular lattice and makes it unstable to melting.

ACKNOWLEDGMENTS

Support by Volkswagen-Stiftung and the Deutsche Forschungsgemeinschaft is gratefully acknowledged. I.L. is also thankful for support by Niedersächsische Ministerium für Wissenschaft und Kultur.

*Corresponding author. Email: pfnuer@fkp.uni-hannover.de

[1] I. Lyuksyutov, A. G. Naumovets, and V. Pokrovsky, *Two-Dimensional Crystals* (Academic Press, New York, 1992).
[2] O. M. Braun and V. K. Medvedev, Usp. Fiz. Nauk **157**, 328 (1989) [Sov. Phys. Usp. **32**, 328 (1989)].
[3] M. S. Gupalo, V. K. Medvedev, B. M. Palyukh, and T. P. Smereka, Fiz. Tverd. Tela **21**, 973 (1979) [Sov. Phys. Solid State **21**, 568 (1979)].
[4] I. F. Lyuksyutov, Zh. Eksp. Teor. Fiz. **89**, 1061 (1985) [Sov. Phys. JETP **62**, 615 (1985)].
[5] D. Jürgens, G. Held, and H. Pfnür, Surf. Sci. **303**, 77 (1994).
[6] V. M. Gavrilyuk and V. K. Medvedev, Fiz. Tverd. Tela **8**, 1811 (1966) [Sov. Phys. Solid State **8**, 1439 (1966)].
[7] T.-M. Lu, G.-C. Wang, and M. G. Lagally, Surf. Sci. **108**, 494 (1981).
[8] J. C. Tracy and J. M. Blakely, Surf. Sci. **15**, 257 (1969).
[9] T. Engel, H. Niehus, and E. Bauer, Surf. Sci. **52**, 237 (1975).
[10] G.-C. Wang and T.-M. Lu, Phys. Rev. B **28**, 6795 (1983).
[11] T. L. Einstein in *Chemistry and Physics of Solid Surfaces VII*, edited by R. Vanselow and R. Howe (Springer, Berlin, 1988), p. 307.
[12] D. A. Huse and M. E. Fisher, Phys. Rev. B **29**, 5031 (1984).
[13] M. E. Fisher, Phys. Rev. **176**, 257 (1968).
[14] G.-C. Wang and T.-M. Lu, Phys. Rev. B **31**, 5918 (1985).
[15] I. F. Lyuksyutov, V. K. Medvedev, and I. N. Yakovkin, Zh. Eksp. Teor. Fiz. **80**, 2452 (1981) [Sov. Phys. JETP **53**, 1284 (1981)].
[16] I. N. Yakovkin, Surf. Sci. **282**, 195 (1993).
[17] T. M. Lu, G.-C. Wang, and M. G. Lagally, Phys. Rev. Lett. **39**, 411 (1977).
[18] D. Kolthoff and H. Pfnür, Surf. Sci. **457**, 134 (2000).
[19] A. G. Naumovets, M. V. Paliy, Yu. S. Vedula, A. T. Loburets, and N. B. Senenko, Prog. Surf. Sci. **48**, 59 (1995).
[20] F. Bagehorn, J. Lorenc, and Cz. Oleksy, Surf. Sci. **349**, 165 (1996).
[21] A. G. Fedorus and A. G. Naumovets, Surf. Sci. **21**, 426 (1970); A. G. Novaco and J. P. McTague, Phys. Rev. B **19**, 5299 (1979).